Catalysis Today 151 (2010) 34–38

Contents lists available at ScienceDirect

Catalysis Today

journal homepage: www.elsevier.com/locate/cattod

Photocatalytic degradation of stearic acid by ZnO thin films and nanostructures deposited by different chemical routes

G. Kenanakis[a,b,c], Z. Giannakoudakis[b], D. Vernardou[a], C. Savvakis[a], N. Katsarakis[a,c,*]

[a] Science Department, School of Applied Technology, Technological Educational Institute of Crete, 710 04 Heraklion, Crete, Greece
[b] Department of Chemistry, University of Crete, 710 03 Heraklion, Crete, Greece
[c] Institute of Electronic Structure and Laser, Foundation for Research & Technology-Hellas, P.O. Box 1385, Vassilika Vouton, 711 10 Heraklion, Crete, Greece

ARTICLE INFO

Article history:
Available online 24 March 2010

Keywords:
Zinc oxide
Nanowires
Photocatalysis
Stearic acid

ABSTRACT

The structural, morphological and photocatalytic properties of ZnO thin films and nanostructures deposited on Corning glass substrates via various chemical routes were investigated. It is demonstrated that the structural and morphological characteristics of the samples depend drastically on deposition technique and parameters. ZnO nanostructured films, nanopetals and nanowires were systematically obtained by varying the experimental conditions. Sol–gel method leads to the formation of dense ZnO nanostructured thin films with a preferred growth orientation along the (0 0 2) crystallographic direction, while ultrasonic spray pyrolysis results in ZnO nanopetals, their dimensions increasing with spraying time. On the other hand, highly oriented ZnO nanowires were obtained via aqueous solution growth on seeded Corning substrates. All ZnO samples show remarkable photocatalytic activity regarding the degradation of stearic acid, which is attributed to their good crystallinity and large surface area. In particular, ZnO nanowires exhibit an outstanding photocatalytic activity, degrading stearic acid by almost 93% in 30 min. This behaviour is mainly due to their high surface-to-volume ratio.

1. Introduction

Heterogeneous photocatalysis on semiconductor surfaces has attracted a lot of attention due to important applications like water disinfection, degradation and complete mineralization of organic contaminants in wastewater, air purification and water splitting for hydrogen production [1–3]. It is mostly titanium dioxide (TiO_2) that has been widely used as a photocatalyst because of its high photocatalytic activity and great thermal, chemical and mechanical stability [4–7].

Zinc oxide (ZnO), on the other hand, is a transparent direct wide band-gap semiconductor ($E_g \sim 3.3$ eV [8]) with a large exciton binding energy (~60 meV [8]), which has been comprehensively studied due to its outstanding properties including piezoelectricity, p-type conductivity and room temperature (RT) ferromagnetism upon appropriate doping, great chemical sensing effects and remarkable photocatalytic activity [8–12]. Besides, it has been reported that ZnO shows better activity than TiO_2 in the photodegradation of some dyes in aqueous solutions since it can absorb more light quanta [11]. However, ZnO undergoes photocorrosion under UV light illumination, which results in a decrease of its photocatalytic activity in aqueous media [13,14].

Recent studies have focussed on the deposition of photoactive TiO_2 thin films on glass substrates [15–19]. There have been up-to-date, however, only few reports on the photocatalytic properties of nanostructured ZnO thin films [20–24]. Moreover, to our knowledge, there has been no systematic study investigating the dependence of the photocatalytic activity of ZnO thin films and nanostructures synthesized by chemical methods on film crystallinity, morphology and thickness.

In this work, we study the photocatalytic activity of ZnO thin films and nanostructures deposited by sol–gel, ultrasonic spray pyrolysis and aqueous solution growth. We attempt to correlate the structural and morphological properties of the as-deposited films and nanostructures with their photocatalytic activity. It is concluded that all nanostructured ZnO thin films show remarkable photocatalytic activity depending mainly on the sample compactness, crystallinity and grain size. In particular, the ZnO nanowires' arrays prepared via aqueous solution growth display an outstanding efficiency in the photodegradation of stearic acid, a fact that is attributed to their high surface-to-volume ratio.

* Corresponding author at: Science Department, School of Applied Technology, Technological Educational Institute of Crete, 710 04 Heraklion, Crete, Greece.
Tel.: +30 2810 379841; fax: +30 2810 379845.
E-mail address: katsan@teicrete.gr (N. Katsarakis).

0920-5861/$ – see front matter © 2010 Elsevier B.V. All rights reserved.
doi:10.1016/j.cattod.2010.02.054

2. Experimental part

2.1. Deposition techniques

ZnO thin films were deposited on square 0.7 mm-thick Corning glass substrates (Corning Eagle 2000 Borosilicate Glass, 10 mm × 10 mm, Specialty Glass Products) by sol–gel and ultrasonic spray pyrolysis. All substrates used were cleaned using a Piranha solution (H_2SO_4/H_2O_2 = 3/1, v/v), rinsed with MilliQ water and dried under N_2 gas flow. Highly oriented ZnO nanowires were grown on Corning glass substrates from aqueous solution according to the approach of Andrés-Vergés et al. [25] and Vayssieres et al. [26]. The substrates used were either bare or pre-coated with six ZnO thin layers deposited by the sol–gel technique (seed).

For the sol–gel procedure [27–29], zinc acetate dihydrate [$Zn(CH_3COO)_2{\cdot}2H_2O$, Aldrich, 99.99%] was first dissolved in a mixture of 2-methoxy ethanol (Sigma–Aldrich, ≥99.5%) and ethanolamine (Sigma–Aldrich, ≥99.0%) at room temperature. The concentration of zinc acetate was 0.75 mol/L and the molar ratio of ethanolamine to zinc acetate was kept at 1:1. The resultant solution was stirred for 1 h at 60 °C to yield a homogeneous, clear and transparent solution using a magnetic stirrer. Consequently, 30 μL of the precursor solution were dropped onto Corning glass substrates, which were then spinned at 2000 rpm for 20 s. After processing, the substrates were baked at 350 °C for 10 min to evaporate the solvent and to remove the organic component in the films. The procedure was repeated for six times. The films were then annealed in air at 450 and 600 °C for 60 min. They were later used as seed layers for the fabrication of ZnO nanowires by aqueous solution growth.

For the ultrasonic spray pyrolysis depositions [30], a 0.5 M aqueous solution of zinc acetate dihydrate [$Zn(CH_3COO)_2{\cdot}2H_2O$, Aldrich, 99.99%] was used as a precursor. A commercial ultrasonic nebulizer (2.4 MHz) generated an aerosol of the precursor solution, which was sprayed vertically through a 4 mm nozzle onto a Corning glass substrate mounted on a heating plate at a distance of 5 cm. High-purity nitrogen was used as the carrier gas, while the spraying rate of the precursor solution was 20 mL/h. The films were deposited in air at a substrate temperature of 450 °C for spraying periods of 30 and 60 min.

ZnO nanostructures were grown via aqueous solution growth (ASG) on Corning glass substrates from an equimolar (0.01 M) aqueous solution of $Zn(NO_3)_2{\cdot}6H_2O$ (Aldrich, 99.999%) and hexamethylenetetramine ($C_6H_{12}N_4$, Sigma–Aldrich, 99.0%) [31,32]. The solution and the substrates, bare or pre-coated with ZnO seed layers prepared via sol–gel, were placed in Pyrex glass bottles with autoclavable screw caps and heated at 95 °C for 5 h in a regular laboratory oven. After the induction period, the samples were thoroughly washed with MilliQ water to eliminate residual salts or amino complexes, and dried in air at the same temperature.

2.2. Characterization techniques

The crystal structure of the ZnO thin films and nanostructures was determined by X-ray diffraction (XRD) using a Rigaku (RINT 2000) diffractometer with Cu Kα X-rays. Their surface morphology was studied with a JEOL JSM-7000F field emission scanning electron microscope (FE-SEM) and an atomic force microscope (AFM) in tapping mode (Digital Instruments—Nanoscope IIIa). The surface area of the sol–gel ZnO samples (1 μm^2 sample surface) was determined by the SPIP version 3.3.5.0 of image metrology, while for the ZnO sample grown via aqueous solution growth at 95 °C, commercial imaging software was applied. The thickness of the films was measured using a stylus profilometer (alpha-step 100, Tencor).

2.3. Photocatalytic activity test

For all photocatalytic performance measurements, stearic acid was used as the organic material to be mineralized. It has been suggested that stearic acid is an appropriate model pollutant for the organic solid films that deposit on (exterior) window glass surfaces [33,34]. Moreover, the decomposition of stearic acid can be demonstrated by FT-IR spectroscopy through the monitoring of the asymmetric C–H stretching mode of the CH_3 group at 2958 cm^{-1} and the asymmetric and symmetric C–H stretching modes of the CH_2 group at 2923 and 2853 cm^{-1}, respectively. The photocatalytic activity experiments on the ZnO thin films and nanostructures for the decomposition of stearic acid (Sigma, 98.5%) were performed at ambient temperature. First, 30 μL of a 0.1 M stearic acid/chloroform solution was spin-coated on the film surface under test at a rotation speed of 500 rpm for 30 s. Samples were then dried at 80 C in air for 10 min. The integrated area of the stearic acid C–H stretching peaks (2800–3000 cm^{-1}) was monitored using a Fourier transform infrared spectrometer (FT-IR, IRPPRESTIGE-21, Shimadzu) before and after light illumination in a box reactor with a UV lamp centred at 365 nm (Philips HPK 125 W, 10 mW/cm^2) at certain time intervals. For ease in comparison of the photocatalytic activity between different samples, the integrated area of the C–H stretching peaks (2800–3000 cm^{-1}) measured at each irradiation time interval was normalized to the initial integrated area (prior to the irradiation) in order to calculate the percentage of stearic acid remaining as a function of irradiation time. Finally, the stearic acid disappearance rate (mol/min) and the formal quantum efficiency (FQE) for all ZnO samples were calculated according to the methodology of Mills and Wang [34].

3. Results and discussion

3.1. Crystallographic data

Fig. 1a depicts X-ray diffraction patterns of ZnO thin films deposited on Corning glass substrates by ultrasonic spray pyrolysis at 450 °C for spraying times of 30 and 60 min. The distance between the spraying nozzle and the substrate was fixed at 5 cm. The films produced are polycrystalline, showing the wurtzite ZnO hexagonal *P*6(3)*mc* structure, while there is no evidence for the presence of other phases. When the spraying time increases from 30 to 60 min, the film thickness rises considerably from 50 nm to 1.4 μm, while at the same time there is a significant change in film's texture. In particular, growth along the (0 0 2) crystallographic direction is favored for 30 min (red solid curve), while for 60 min the (1 0 1), (1 0 2), (1 0 3) and (1 1 2) diffraction peaks evolve too (light-blue dotted curve).

Fig. 1b displays the X-ray diffraction patterns of 140 nm-thick ZnO films fabricated by sol–gel at 450 °C (red solid line) and 600 °C (green dotted line) on Corning glass. It can be readily observed that, in this case, only the (0 0 2) diffraction peak occurs, demonstrating that there is a preferred growth orientation along the *c*-axis, i.e., perpendicular to the substrate. In Fig. 1c, X-ray diffraction patterns of ZnO nanostructures deposited on Corning glass substrates by aqueous solution growth for 5 h are presented. The substrates used were either bare (green dotted line) or pre-coated with a 140 nm-thick ZnO seed layer deposited by the sol–gel technique at 450 °C (magenta solid curve). It can be readily seen that, if no seed layer is applied onto the Corning glass substrates prior to the aqueous solution growth, all reflections corresponding to the hexagonal wurtzite *P*6(3)*mc* structure (JCPDS card file No. 36-1451) are present and there is no preferential growth orientation (green dotted line). On the other hand, when a 140 nm-thick ZnO seed layer is applied onto the Corning glass substrates prior to the aqueous solution growth,

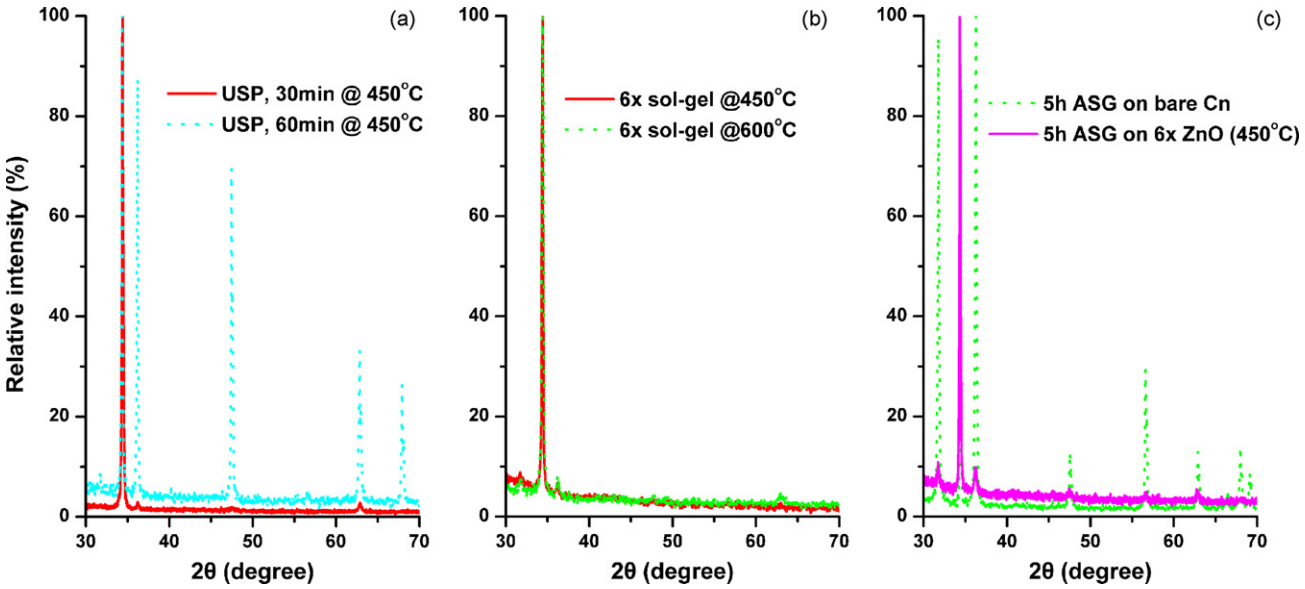

Fig. 1. (a) XRD patterns of ZnO nanostructured thin films grown on Corning glass by ultrasonic spray pyrolysis for 30 min (red curve) and 60 min (light-blue dotted curve) at 450 °C, (b) six-layered (6×) ZnO thin films grown on Corning glass substrates by sol–gel at 450 °C (red curve) and 600 °C (green dotted curve) and (c) ZnO nanostructures produced by aqueous solution growth at 95 °C for 5 h on bare Corning glass (green dotted curve) and Corning glass with a 140 nm-thick ZnO seed layer (450 °C) on top (magenta curve). (For interpretation of the references to color in this figure legend, the reader is referred to the web version of the article.)

there is a clear preferential growth orientation of the ZnO nanostructured samples along the (0 0 2) crystallographic direction, i.e., perpendicular to the Corning glass substrates (magenta solid line).

3.2. Scanning electron microscopy (SEM)

Fig. 2a and b shows SEM micrographs of ZnO samples deposited on Corning glass substrates by ultrasonic spray pyrolysis at 450 °C for 30 and 60 min. For 30 min growth, ZnO nanopetals occur, having a thickness of ~25 nm and a length of ~100–150 nm (see the inset of Fig. 2a). Some nanowires of ~20 nm diameter, emerging perpendicular to the substrate can also be observed. For 60 min spraying time, the nanopetals grow substantially reaching a length of ~1–2 μm, while their thickness remains almost unaffected. In Fig. 2c, a SEM micrograph of a 140 nm-thick, six-layered ZnO film fabricated by sol–gel at 450 °C is depicted. The film is quite dense showing uniform grains with a diameter of ~40 nm. The grain size increases with substrate temperature, reaching ~90 nm for 600 °C.

Fig. 2d, e and f depict SEM micrographs of ZnO nanostructures deposited by aqueous solution growth at 95 °C on Corning glass substrates for 5 h. As it can be observed, if no seed layer is applied (Fig. 2d), flowerlike microstructures occur, consisting of uniform nanorods with a diameter ranging from 400 to 500 nm and length of several microns (~5–6 μm). All nanorods have hexagonal cross-

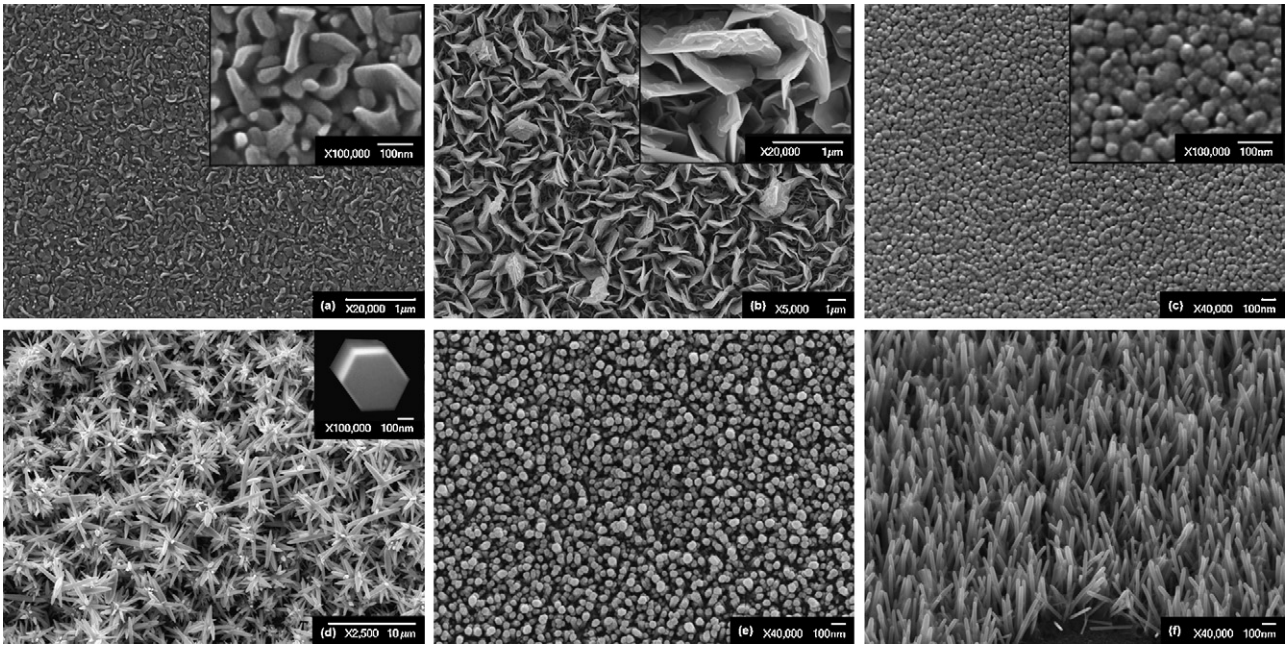

Fig. 2. SEM images of (a), (b) ZnO samples grown on Corning glass by ultrasonic spray pyrolysis at 450 °C for 30 and 60 min, respectively, (c) 140 nm-thick ZnO thin film grown on Corning glass by sol–gel at 450 °C, (d)–(f) ZnO nanostructures produced by aqueous solution growth at 95 °C for 5 h on either bare Corning glass substrates (d), or Corning glass pre-coated with a 140 nm-thick ZnO seed layer (450 C) [(e) top view and (f) side view].

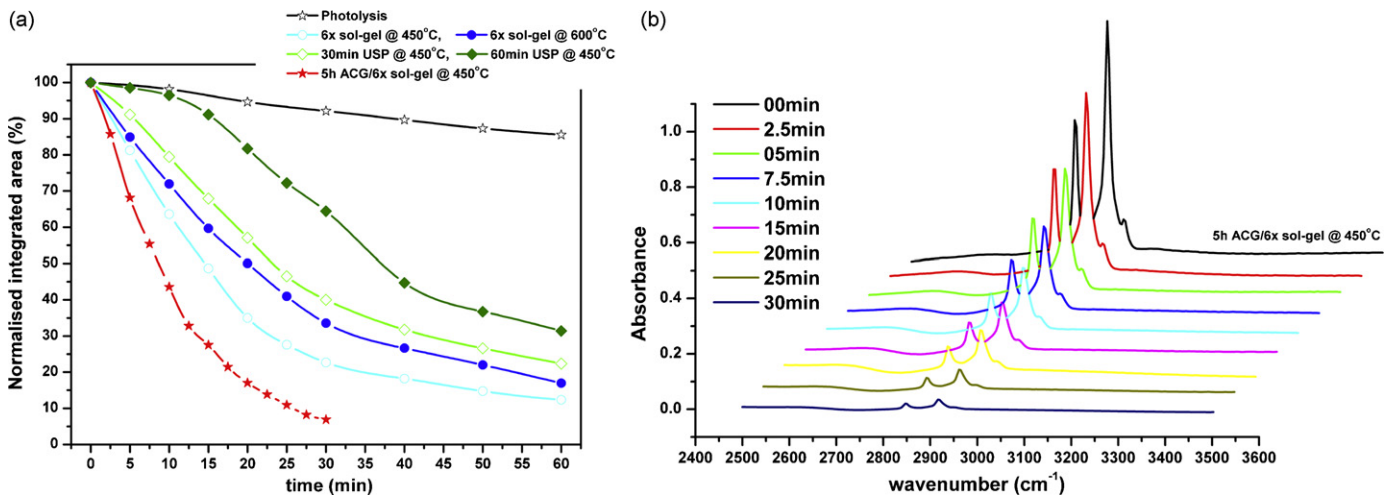

Fig. 3. (a) Normalized integrated area vs. irradiation time for (i) ZnO thin films deposited by ultrasonic spray pyrolysis at 450 °C for 30 min (light-green open squares) and 60 min (dark-green closed squares), (ii) 140 nm-thick ZnO thin films deposited by sol–gel at 450 °C (light-blue open circles) and 600 °C (dark-blue closed circles) and (iii) ZnO nanowires prepared via aqueous solution growth at 95 °C on seeded Corning glass substrates (red stars). For comparison reasons, the photolysis curve (black open stars) is also presented. (b) FT-IR absorption spectra demonstrating the degradation of stearic acid on the ZnO nanowires' array vs. irradiation time. (For interpretation of the references to color in this figure legend, the reader is referred to the web version of the article.)

section (see the inset of Fig. 2d), implying the occurrence of the wurtzite ZnO crystal structure as it was also demonstrated by XRD (see Fig. 1c). On the other hand, when a 140 nm-thick seed layer is applied onto the substrate, well-aligned, *c*-axis oriented ZnO nanowires are formed (see Fig. 2e and f). The nanowires' diameter is ~40 nm, while their length ranges from 400 to 500 nm (aspect ratio ~10–12.5). The nanowires emerge perpendicular to the substrate applied, are quite dense and uniform, while they all display a hexagonal cross-section. These remarks are in agreement with the XRD results which clearly demonstrate that the ZnO samples deposited by aqueous solution growth on pre-coated Corning glass substrates exhibit a preferential growth orientation along the (0 0 2) direction (see magenta line in Fig. 1c).

3.3. Photocatalytic properties

Fig. 3a presents the normalized integrated area vs. irradiation time curves for all ZnO samples fabricated by different chemical routes, while in Fig. 3b the FT-IR absorption spectra of the ZnO nanowires' array deposited via aqueous solution growth on a seeded Corning glass substrate at 95 °C are displayed vs. irradiation time. It can be noticed that all ZnO thin films and nanostructures show remarkable photocatalytic activity, degrading stearic acid by more than 50% at 60 min. This is most probably due to their good crystallinity and large surface area (see Table 1). In particular, ZnO nanowires synthesized via aqueous solution growth show an outstanding photocatalytic activity, degrading stearic acid by ~93.12% at 30 min. This behaviour is mainly attributed to the high surface-to-volume ratio of the ZnO nanowires' arrays (surface area 53.11 μm^2, Table 1). For comparison reasons, the photolysis curve (no catalyst present) is also displayed in Fig. 3a (black open stars). It can be seen that the UV-A light (365 nm) results only in ~14.47% degradation of stearic acid after 60 min of exposure.

The photocatalytic activity of all ZnO samples deposited by chemical routes at 30 min is summarized in Table 1, where the stearic acid disappearance rate (mol/min) and the formal quantum efficiency (FQE) are also displayed. It can be observed that ZnO thin films deposited by sol–gel at 450 °C show better activity (77.33%, FQE = 1.58×10^{-3}) than those grown at 600 °C (66.43%, FQE = 1.41×10^{-3}). This is possibly due to larger surface area, which is in turn related to smaller grain size. In fact, ZnO thin films deposited by sol–gel at 450 °C exhibit a grain size of ~40 nm (surface area 0.5 μm^2, Table 1), while at 600 °C the grain size rises to ~90 nm (surface area 0.41 μm^2, Table 1). ZnO samples prepared via ultrasonic spray pyrolysis show better photocatalytic activity for smaller spraying times. Specifically, ZnO thin films deposited after 30 min spraying time, exhibit an activity of ~60% (FQE = 0.39×10^{-3}), while the ones deposited after 60 min show an activity of only 35.6% (FQE = 0.06×10^{-3}). This is attributed to the much smaller nanopetals observed for the samples grown for 30 min, compared with those occurring after 60 min growth (see Fig. 2a and b). Finally, ZnO nanowires grown via aqueous solution growth at 95 °C on Corning glass substrates pre-coated with a 140 nm-thick ZnO seed layer show by far the best photocatalytic activity and FQE, degrading stearic acid by almost 93.12% at 30 min (FQE = 4.77×10^{-3}). The high aspect ratio of the nanowires formed (~10–12.5), together with their enhanced crystallinity results in this significant photocatalytic activity.

Table 1
Thickness, surface area (1 μm^2 sample surface), photocatalytic activity at 30 min, initial stearic acid disappearance rate (mol/min) and formal quantum efficiency (FQE, see Mills and Wang [34]) for the ZnO samples deposited via chemical methods.

	Photolysis	USP 30 min, 450 °C	USP 60 min, 450 °C	Sol–gel 6×, 450 °C	Sol–gel 6×, 600 °C	ASG 5 h on 6× sol–gel, 450 °C
Thickness (nm)	–	50	1400	140	140	500
Surface area (μm^2)	–	[a]	[a]	0.50	0.41	53.11
α (%) at 30 min	7.85%	60.00%	35.60%	77.33%	66.43%	93.12%
Initial SA disappearance rate (mol/min)	4.44×10^{-10}	3.68×10^{-9}	5.65×10^{-10}	1.49×10^{-8}	1.33×10^{-8}	4.5×10^{-8}
Formal quantum efficiency $(FQE)_{(SA)}/10^{-3}$	0.047	0.39	0.06	1.58	1.41	4.77

[a] It was not possible to measure the surface area of the ZnO samples grown via ultrasonic spray pyrolysis. These samples do not have a flat surface, are quite rough compared to the sol–gel ones and it was therefore impossible to perform AFM measurements on them.

4. Conclusions

ZnO thin films and nanostructures were obtained by sol–gel, ultrasonic spray pyrolysis and aqueous chemical growth. All samples show very good crystallinity, while their texture and morphology depend strongly on the deposition technique and the experimental parameters, i.e., growth time, temperature, occurrence of a seed layer. Sol–gel method leads to *c*-axis oriented, dense, nanostructured thin films. Their grain size increases with deposition temperature. Ultrasonic spray pyrolysis results in ZnO thin films consisting of nanopetals, their dimensions increasing drastically with spraying time. On the other hand, aqueous solution growth on seeded Corning glass substrates leads to the formation of *c*-axis oriented ZnO nanowires, whose diameter depends on the grain size of the seed layer used. All ZnO samples show remarkable photocatalytic activity regarding the degradation of stearic acid. This behaviour is due to their good crystallinity and large surface area. In particular, ZnO nanowires' arrays exhibit significant photocatalytic activity, which is mainly attributed to their high surface-to-volume ratio.

Acknowledgements

The authors would like to acknowledge Dr. Emmanuel Spanakis for fruitful comments and discussions and the financial support by the EU project ENSEMBLE.

References

[1] M.R. Hoffmann, S.T. Martin, W.Y. Choi, D.W. Bahnemann, Chem. Rev. 95 (1995) 69.
[2] A. Mills, S. LeHunte, J. Photochem. Photobiol. A: Chem. 108 (1997) 1.
[3] D.A. Tryk, A. Fujishima, K. Honda, Electrochim. Acta 45 (2000) 2363.
[4] A. Fujishima, T.N. Rao, D.A. Tryk, J. Photochem. Photobiol. C: Photochem. Rev. 1 (2001) 1.
[5] K. Rajeshwar, M.E. Osugi, W. Chanmanee, C.R. Chenthamarakshan, M.V.B. Zanoni, P. Kajitvichyanukul, R. Krishnan-Ayer, J. Photochem. Photobiol. C: Photochem. Rev. 9 (2008) 15.
[6] K. Hashimoto, H. Irie, A. Fujishima, Jpn. J. Appl. Phys. 44 (2005) 8269.
[7] O. Carp, C.L. Huisman, A. Reller, Prog. Solid State Chem. 32 (2004) 33.
[8] Ü. Özgür, Y.I. Alivov, C. Liu, A. Teke, M.A. Reshchikov, S. Doğan, V. Avrutin, S.J. Cho, H. Morkoç, J. Appl. Phys. 98 (2005) 041301.
[9] D.P. Norton, Y.W. Heo, M.P. Ivill, K. Ip, S.J. Pearton, M.F. Chisholm, T. Steiner, Mater. Today 7 (6) (2004) 34.
[10] L. Schmidt-Mende, J.L. MacManus-Driscoll, Mater. Today 10 (5) (2007) 40.
[11] S. Sakthivel, B. Neppolian, M.V. Shankar, B. Arabindoo, M. Palanichamy, V. Murugesan, Sol. Energy Mater. Sol. Cells 77 (2003) 65.
[12] Y.J. Jang, C. Simer, T. Ohm, Mater. Res. Bull. 41 (2006) 67.
[13] C. Hariharan, Appl. Catal. A: Gen. 304 (2006) 55.
[14] P. Spathis, I. Poulios, Corrosion Sci. 37 (1995) 673.
[15] D.S. Tsoukleris, A.I. Kontos, P. Aloupogiannis, P. Falaras, Catal. Today 124 (2007) 110.
[16] H. Choi, E. Stathatos, D.D. Dionysiou, Thin Solid Films 510 (2006) 107.
[17] P. Evans, D.W. Sheel, Surf. Coat. Technol. 201 (2007) 9319.
[18] Y. Chen, D.D. Dionysiou, Appl. Catal. B: Environ. 62 (2006) 255.
[19] A. Mills, G. Hill, S. Bhopal, I.P. Parkin, S.A. O'Neill, J. Photochem. Photobiol. A: Chem. 160 (2003) 185.
[20] J.L. Yang, S.J. An, W.I. Park, G.C. Yi, W. Choi, Adv. Mater. 16 (2004) 1661.
[21] F. Xu, Z.-Y. Yuan, G.-H. Du, T.-Z. Ren, C. Bouvy, M. Halasa, B.-L. Su, Nanotechnology 17 (2006) 588.
[22] F. Xu, G.-H. Du, M. Halasa, B.-L. Su, Chem. Phys. Lett. 426 (2006) 129.
[23] B. Pal, M. Sharon, Mater. Chem. Phys. 76 (2002) 82.
[24] F. Peng, H. Wang, H. Yu, S. Chen, Mater. Res. Bull. 41 (2006) 2123.
[25] M. Andrés-Vergés, A. Mifsud, C.J. Serna, J. Chem. Soc., Faraday Trans. 86 (1990) 959.
[26] L. Vayssieres, K. Keis, S.-E. Lindquist, A. Hagfeldt, J. Phys. Chem. B 105 (2001) 3350.
[27] H. Li, J. Wang, H. Liu, H. Zhang, X. Li, J. Cryst. Growth 275 (2005) e943.
[28] J. Qiu, Z. Jin, Z. Liu, X. Liu, G. Liu, W. Wu, X. Zhang, X. Gao, Thin Solid Films 515 (2007) 2897.
[29] J. Zhao, Z.-G. Jin, T. Li, X.-X. Liu, J. Eur. Ceram. Soc. 26 (2006) 2769.
[30] H.-W. Suh, G.-Y. Kim, Y.-S. Jung, W.-K. Choi, D. Byun, J. Appl. Phys. 97 (2005) 044305.
[31] D. Vernardou, G. Kenanakis, S. Couris, E. Koudoumas, E. Kymakis, N. Katsarakis, Thin Solid Films 515 (2007) 8764.
[32] G. Kenanakis, D. Vernardou, E. Koudoumas, G. Kiriakidis, N. Katsarakis, Sens. Actuators B: Chem. 124 (2007) 187.
[33] P. Evans, S. Mantke, A. Mills, A. Robinson, D.W. Sheel, J. Photochem. Photobiol. A: Chem. 188 (2007) 387.
[34] A. Mills, J. Wang, J. Photochem. Photobiol. A: Chem. 182 (2006) 181.